Hybrid polymer–metal oxide thin films for photovoltaic applications†

Johann Bouclé,[ab] Punniamoorthy Ravirajan[ac] and Jenny Nelson*[a]

Received 30th April 2007, Accepted 25th May 2007
First published as an Advance Article on the web 18th June 2007
DOI: 10.1039/b706547g

We review progress in the development of organic–inorganic hybrid photovoltaic materials consisting of a conjugated polymer as an electron donor and a nanocrystalline metal oxide as the electron acceptor. We distinguish two main approaches: (1) where a rigid porous metal oxide structure is filled with polymer and (2) where metal oxide nanoparticles and polymer are co-deposited from solution to form a blend film. In the case of porous structures, performance is limited by the infiltration of polymer into the pores of the metal oxide and control of the nanostructure dimensions. In the case of blends, control of the blend morphology and transport between nanoparticles are limitations. In both cases, further improvements are possible by modifying the metal oxide organic interface to optimise charge transfer, by improving both inter- and intra-particle transport within the metal oxide phase, for example by the use of single crystalline nanorods, and by optimising the choice of electrode materials. Though unlikely to achieve the highest photocurrents, the polymer–metal oxide composites provide a model system to study the effects of interface properties and film morphology on the performance of bulk heterojunction photovoltaic devices.

Introduction

Low-cost semiconductor materials and facile fabrication routes for photovoltaic (PV) junctions have been longstanding goals of photovoltaic materials research. New materials or fabrication procedures that could reduce the cost of photovoltaic electricity substantially could help to drive a rapid expansion in implementation of photovoltaic technology. Molecular semiconductors such as conjugated polymers, small molecules and dyes, are particularly interesting for this purpose, largely because of the potential for processing such materials directly from solution, and so enabling low-cost manufacture of large-area thin semiconductor films. Additional advantages are compatibility with flexible substrates and the potential to vary the colour of photovoltaic modules by altering the chemical structure, as well as advantages in module performance at low light levels or raised temperatures.

The last decade has seen an explosion of academic and industrial interest in the PV applications of molecular thin films, following the demonstration of high photon-to-electron quantum efficiencies for donor–acceptor heterojunctions involving a molecular light absorber.[1,2] The heterojunction supplies, by means of the difference in ionisation potential and electron affinity of the two materials, the driving force for charge separation that is necessary to dissociate the tightly bound photogenerated exciton into separate charges. High photocurrent quantum efficiency requires a high probability of

[a]*Department of Physics, Imperial College London, London, UK SW7 2BW. E-mail: jenny.nelson@imperial.ac.uk*
[b]*Cavendish Laboratory, University of Cambridge, J. J. Thomson Avenue, Cambridge, UK CB3 0HE*
[c]*Department of Physics, University of Jaffna, Jaffna, Sri Lanka*
† This paper is part of a *Journal of Materials Chemistry* theme issue on New Energy Materials. Guest editor: M. Saiful Islam.

Johann Bouclé

Johann Bouclé studied Physics in France where he completed his PhD on the development of hybrid nanocomposites SiC–polymer for electro-optical applications, both in the University of Le Mans (LPEC) and in the CEA/Saclay (SPAM). He joined Jenny Nelson and Donal Bradley's group at Imperial College London (UK) in 2005 as a postdoctoral research associate, where he developed hybrid bulk-heterojunction solar cells. He is currently working in Neil Greenham's group (Cambridge, UK) on nanostructured hybrid solar cells.

Punniamoorthy Ravirajan

Punniamoorthy Ravirajan received a doctorate degree in Physics under the supervision of Prof. Jenny Nelson and Prof. Donal D. C. Bradley at Imperial College London (UK) in 2004. After a postdoctoral period with them, he returned to University of Jaffna, Sri Lanka, where he was appointed lecturer in Physics in 1996, and senior lecturer in 2005. Over the six years, his main research activities have been in optimisation of hybrid metal oxides–polymer photovoltaic devices.

exciton generation close to a donor–acceptor interface, and this is achieved by means of a dispersed or bulk heterojunction, where the two components are combined in such a way that the interface is highly reticulated and presents a very large area compared to the geometrical area of the device. Typically, the domain sizes within either component of the heterojunction should be comparable to the diffusion length of an exciton in that material. For soluble media, the large interfacial area is achieved spontaneously by blending the acceptor and donor components together in a solution, which is then cast into thin films. With vacuum-deposited molecular films, the large interface can be achieved by co-evaporation of the donor and acceptor type molecules. When a photon is absorbed in either of the materials in such a bulk heterojunction, the exciton so created will dissociate into separate charges if it diffuses to the interface before it relaxes. If the composite film is enclosed between two electrodes with asymmetric affinities for electrons and holes, the separated charges can then be collected to generate a photocurrent (Fig. 1).

Organic solar cell research has focused on the characterisation of new materials or combinations of materials, optimisation of device design, and optimisation of device performance through processing. Research has focused on the use of fullerenes and fullerene derivatives as acceptors, because of the high charge mobilities in these materials and their high electron affinities compared to other molecular acceptors. In particular the combination of poly-3-hexylthiophene (P3HT, see Scheme 1 for the chemical structure) with C_{60} derivatives has resulted in the highest power-conversion efficiencies of any type of polymer-based solar cell (4–5%), and has been the focus of intense interest.[3,4] Blends of two polymers,[1,5] or of other molecular donor and acceptor materials[6] have also shown promising performance, although not yet exceeding polymer–fullerene-based devices.

An alternative type of donor–acceptor heterojunction device to polymer–fullerene and polymer–polymer systems consists of an organic semiconductor as donor and an inorganic semiconductor component, such as a II–VI compound semiconductor or a metal oxide, as the electron acceptor. Such structures are often referred to as 'hybrid' devices. Crystalline and nanocrystalline inorganic semiconductors have several attributes as electron acceptors, including relatively high electron mobility, high electron affinities, and good physical and chemical stability. Solution-processible nanocrystalline semiconductors that can be prepared in different morphologies offer the potential for a large area interface when combined with a solution-processed organic component. Hybrid polymer–inorganic structures can be prepared in different ways: a planar *bilayer* structure where an organic layer is deposited on top of an inorganic semiconductor layer; nanostructured *porous* structures where a connected semiconductor layer is filled with a conjugated polymer; and *blends* of nanocrystals with polymer where semiconductor nanoparticles and polymer are deposited from the same solution (Fig. 1). The inorganic semiconductors studied for hybrid devices have included II–VI and I–III–VI compound semiconductors, which, critically, also offer optical absorption in the red part of the spectrum,[7] metal

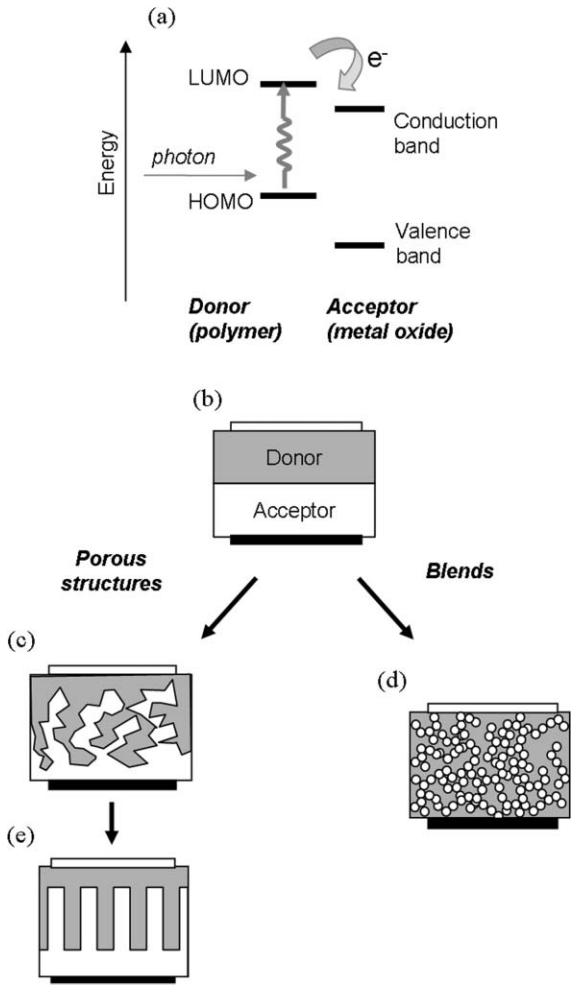

Fig. 1 (a) Energy-level diagram of photoinduced electron transfer at a polymer–metal oxide interface. Absorption of a photon in the polymer creates an exciton, which then dissociates by transferring an electron to the metal oxide, if the exciton is generated close to the interface. (b)–(e) Types of polymer–metal oxide donor–acceptor heterojunctions. (b) A bilayer heterojunction. (c) A heterojunction based on a porous acceptor phase filled with donor. (d) A heterojunction based on nanoparticles dispersed in a donor matrix. (e) An 'ideal' heterojunction containing vertically aligned domains. In cases (b), (c) and (e), charges separated at the interface are helped to the opposite electrodes by diffusion, while in (d) charges separated at the interface rely on differences in the work function of the electrodes for direction of the photocurrent.

Jenny Nelson

Jenny Nelson is a Professor of Physics at Imperial College London (UK), where she has researched novel types of solar cell since 1989. Her current research focuses on photovoltaic energy conversion using molecular materials and the modelling of charge transport in organic semiconductors. She has published around 100 papers on photovoltaic materials and devices, and a book on the physics of solar cells.

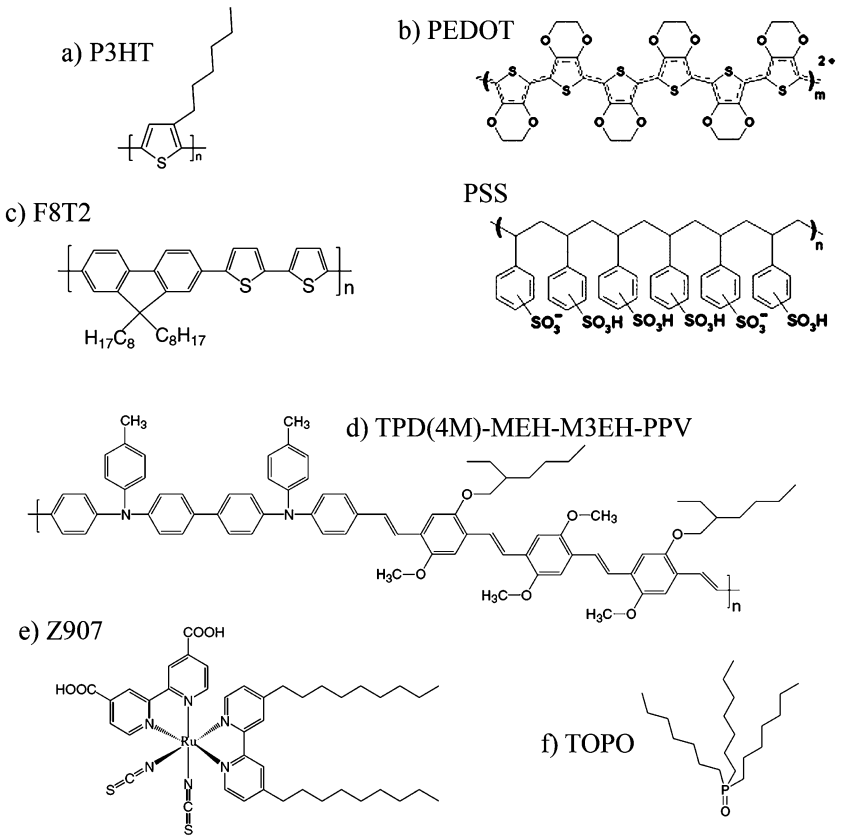

Scheme 1 Chemical structures of some of the polymers and molecules used: (a) poly-3-hexylthiophene (P3HT), (b) poly-(3,4-ethylenedioxythiophene)–poly(styrenesulfonate) (PEDOT–PSS), (c) poly-(9, 9′-dioctylfluorene-co-bithiophene) (F8T2), (d) poly[(1,4-phenylene-(4-methylphenyl)amino-4,4′-diphenylene-(4-methylphenyl)amino-1,4-phenylene-ethenylene-2-methoxy-5-(2-ethylexyloxy)-1,4-phenylene-ethenylene)-co-(2,5-dimethoxy-1,4-phenylene-ethenylene-2-methoxy-5-(2-ethylhexyloxy)-1,4-phenylene-ethenylene)] TPD(4M)–MEH–M3EH–PPV terpolymer,[19] (e) amphiphilic polypyridyl ruthenium complex (Z907) *cis*-RuLL′(SCN)$_2$ (L = 4,4′-dicarboxylic acid-2,2′-bipyridine, L′ = 4,4′-dinonyl-2,2′-bipyridine),[64] and (f) trioctylphosphine oxide (TOPO).

oxide semiconductors (reviewed herein), and thin film or nanocrystalline silicon.[8] Although the highest power-conversion efficiencies to date have been achieved with II–VI nanocrystalline semiconductors, in this paper we will focus on the use of polymer–metal oxide hybrids. This group of materials is of particular interest because of the wide range of morphologies in which the semiconductor can be prepared. Control of morphology *via* wet chemical synthetic methods means that the same material can be prepared in forms ranging from dense layer to dispersed nanocrystal to rigid connected nanostructures, offering a valuable perspective into the role of morphology in the photovoltaic action of bulk heterojunctions. In addition, metal oxides offer optical properties that mean they can be used to enhance light trapping, they are cheap and non-toxic, and enjoy a large experience base from research into photocatalysis, gas sensors, and dye-sensitised solar cells. Titanium dioxide (TiO_2) in particular has been widely studied for hybrid organic–inorganic solar cells. Zinc oxide (ZnO) is an alternative that offers a very high electron mobility and high electron affinity.

Nanostructured TiO_2 has been studied as a photovoltaic material since the 1980s, when the first observations of efficient photoinduced charge injection from dyes into TiO_2 were reported,[9] establishing the basis for dye-sensitised solar cells.[10] The sensitisation of TiO_2 by conjugated polymers or molecular films rather than by chemically adsorbed dye monolayers became of interest in the late 1990s following the first reports of photocurrent generation from conjugated polymer-based heterojunctions. Several studies established that efficient photoinduced electron transfer from conjugated polymers into TiO_2 was possible.[11–14] Relative to dye-sensitised solar cells, a solid nanostructured TiO_2–polymer solar cell offers the potential advantage of useful photocurrents at much smaller device thicknesses, because the entire polymer-filled pore volume is available for exciton generation, rather than only a dye monolayer at the TiO_2 surface. Relative to all-organic polymer–fullerene or polymer–polymer structures, the design offers rigidity and hence mechanical stability of the nanostructure. The first reports of hybrid polymer–TiO_2 photovoltaic devices[13,15,16] showed that photocurrent generation (albeit modest) could be achieved; and that bilayer, porous nanostructured and blend structures could all be exploited. These early studies soon established that structuring of the TiO_2–polymer interface leads to increased photocurrents relative to a bilayer structure with a planar interface (Fig. 2),[15,17] so establishing the key role of the metal oxide–polymer interface morphology.

In this paper, we first review the current status of hybrid polymer–metal oxide devices based on both porous structures and blends. Then, for each of these two groups of

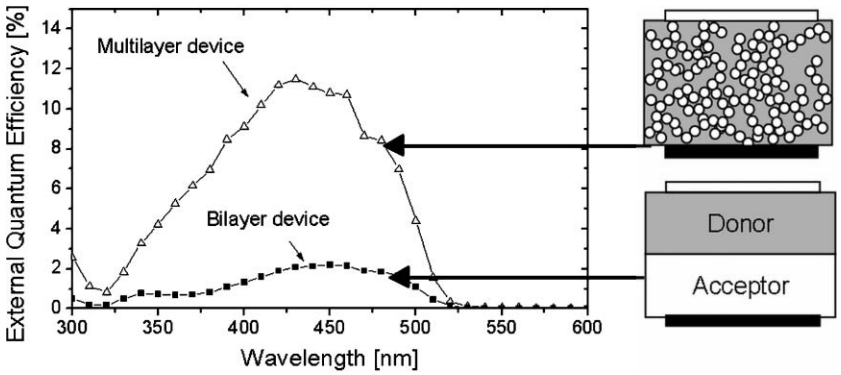

Fig. 2 External quantum efficiency spectra of an ITO/dense TiO_2/porous TiO_2/F8T2 polymer/Au device (triangles) in comparison with a bilayer device containing no porous TiO_2 layer (squares). Reprinted with permission from ref. 17. Copyright (2004) American Institute of Physics.

hybrid structure, we identify the main challenges to improved performance and discuss the strategies to address those challenges.

Status of hybrid polymer–metal oxide photovoltaic devices

Hybrid devices based on polymer–porous metal oxide structures

Studies of conjugated polymer–porous TiO_2 structures have focused on optimisation of the layer structure of the device and choice of polymer materials. By optimisation of the device thickness and electrode choice, groups achieved photocurrent external quantum efficiency (EQE) values of 10,[18] 23,[15] and 40%.[19] Key steps in these optimisations were the reduction of the polymer and TiO_2 layer thicknesses to the region of 50–100 nm; the use of thin dip- or spin-coated nanocrystalline TiO_2 layers; and the choice of polymer, in terms of its exciton-diffusion length, mobility and optical absorption.

A key factor in achieving high power-conversion efficiency (PCE) as well as high EQE is the choice of electrode materials. In porous polymer–metal oxide structures the metal oxide acceptor layer is normally deposited on top of a transparent conducting oxide-coated glass substrate, and an evaporated metal is deposited on top of the active layers as a hole-collecting contact. This polarity is the opposite of most commonly reported organic solar cell structures where the conducting oxide (usually indium tin oxide (ITO)) acts as the hole-collecting electrode. Since the work function of ITO (4.5–4.7 eV) is intermediate between typical HOMO and LUMO values for organic photovoltaic materials, ITO can, in principle, collect either electrons or holes. If the ITO is not insulated from the donor material in the polymer–metal oxide structure, then charge leakage occurs and the device current–voltage (J–V) characteristic suffers a low fill factor. The opposite electrode should have a sufficiently high work function to collect holes from the donor material. A high work function electrode can be provided by a layer of a doped conducting polymer such as PEDOT–PSS under the metal top contact[19] or a high work function metal such as platinum.[17] Poor matching of the anode work function and donor HOMO level leads to a sigmoidal J–V curve characteristic of a low conductivity interface and (again) a low fill factor.[20] The anode selectivity can be further improved using donor material to insulate the contact from the metal oxide. Fig. 3 demonstrates the effects on device J–V characteristics of a porous polymer–TiO_2 structure of a dense TiO_2 hole-blocking layer between polymer and ITO, and of a spin-coated polymer (electron blocking) layer between metal oxide and top electrode. The highest power-conversion efficiency for a polymer–porous metal oxide structure of 0.58% was achieved

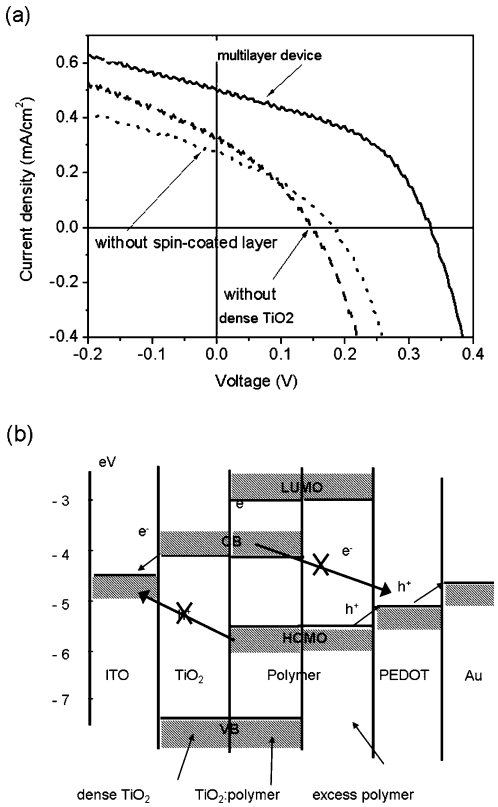

Fig. 3 (a) J–V characteristics of an ITO/dense TiO_2/porous TiO_2/dip-coated polymer/spin-coated polymer/PEDOT–PSS/Au device (solid line), in comparison with J–V characteristics equivalent devices where the dense TiO_2 (dashed line) and the spin-coated polymer layer (dotted line) have been removed. (b) Proposed electronic energy-level diagram for the devices. The dense TiO_2 layer serves to block hole transfer from polymer to TiO2, while the spin-coated polymer layer serves to block electron transfer to the top electrode. Both layers thus prevent shunt pathways.

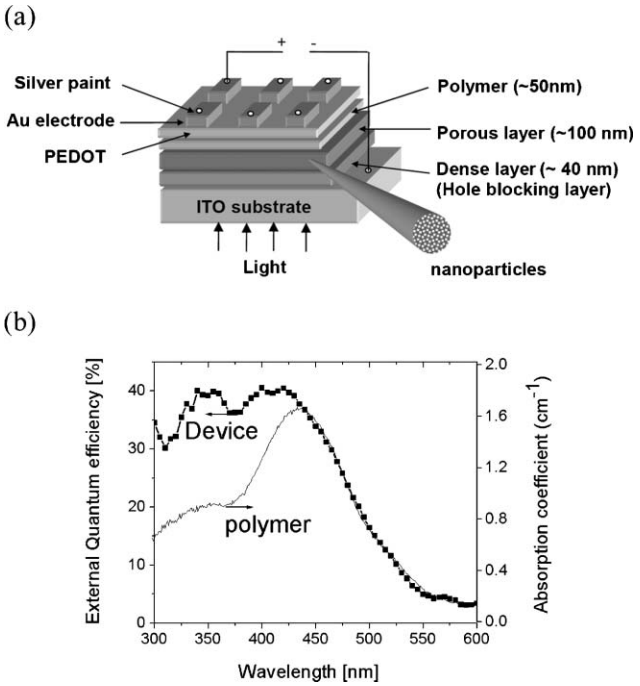

Fig. 4 (a) Schematic of the device structure of a multilayer polymer–porous metal oxide device, incorporating a dense oxide layer and a polymer layer to improve electrode selectivity. (b) Quantum efficiency spectrum (symbols) of a multilayer polymer–porous metal oxide device made from polymer and TiO_2, and the corresponding absorption spectrum of the TPD (4M)–MEH–M3EH–PPV polymer (solid line). Reprinted with permission from ref. 19. Copyright (2005) American Institute of Physics.

for a multilayer device structure incorporating both these buffer layers and suitable electrode materials (Fig. 4).[19]

Hybrid devices based on polymer–nanocrystal blends

In the case of porous metal oxide–polymer systems, the complete infiltration of the porous oxide electrode by a conjugated polymer remains one of the main challenges in achieving efficient photovoltaic devices. In this context, polymer–nanocrystal blends, which can be processed from solution in a single step, offer the advantage of an improved organic–inorganic interface, as well as of potential control over the morphologies and physical properties of the semiconducting nanocrystals.[21] Easily synthesised through chemical methods in solution, high electron affinity nanoparticle and quantum dots of various nature have been incorporated successfully into organic semiconductors of relatively low ionisation potential, favouring charge transfer at the organic–inorganic interface. Typical blend device architecture is presented in Fig. 5(a).

In the development of hybrid blend systems for photovoltaics, most attention has focused on light-absorbing nanoparticles made from II–VI semiconductors such as CdSe and PbS. These materials offer long wavelength absorption, the extent of which can be tuned through control of the nanoparticle size. In particular, photovoltaic devices based on CdSe nanoparticles and P3HT polymer have demonstrated power-conversion efficiencies up to 1.7% under global AM 1.5

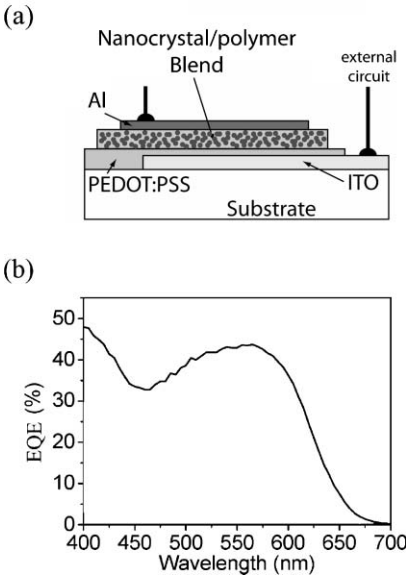

Fig. 5 (a) Typical structure of hybrid nanocrystal–polymer blend photovoltaic devices. (b) External quantum efficiency spectrum of a state-of-the-art blend system based on CdSe branched particles and alternating polyfluorene co-polymer (red-APFO) processed from *p*-xylene, associated with 2.4% efficiency under simulated solar irradiation (AM1.5 Global). Reprinted with permission from ref. 24. Copyright (2006) American Chemical Society.

simulated illumination.[22] Studies on such systems have explored the role of the organic ligand located at the particle surface,[7] and of the blend morphology and nanoparticle shape. Replacing the nanoparticles with three-dimensional nanocrystal structures to improve electron percolation, led to power-conversion efficiencies of 2.1% and above (AM 1.5, 100 mW cm^{-2}) for blends of CdSe tetrapods and a poly(*p*-phenylenvinylene) derivative (OC_1C_{10}–PPV).[23] Further improvements have been obtained by using a red polyfluorene co-polymer, resulting in an extended spectral response out to 650 nm and power-conversion efficiencies of up to 2.4% [Fig. 5(b)].[24] Blend devices incorporating narrow band gap nanocrystals, such as PbSe, in semi-conducting polymers offer further improvements in photocurrent by harnessing near infrared photons.[25]

In this paper, we focus on hybrid devices using nanostructured metal oxides such as TiO_2 and ZnO as the acceptor component. These materials avoid the use of toxic components such as Cd or Pb. Photocurrents are lower than achieved with II–VI nanoparticles on account of the high optical gap of the metal oxides used. Nevertheless, promising blend devices have been demonstrated; an AM1.5 power-conversion efficiency of 1.4% was reported for hybrid blend devices based on zinc oxide (ZnO) nanoparticles (5 nm) with a poly-[2-methoxy-5-(3′,7′-dimethyloctyloxy)-1,4-phenylenevinylene] (MDMO–PPV) polymer.[26] Device efficiencies have been reported recently for blends of isotropic TiO_2 particles with P3HT (PCE = 0.42%, AM1, 100 mW cm^{-2}),[27] and elongated TiO_2 rods in poly[2-methoxy-5-(2′-ethylhexyloxy)-1,4-phenylenevinylene] MEH–PPV (PCE = 0.49%, AM1.5, 100 mW cm^{-2}).[28]

Strategies to improve porous oxide–polymer materials and devices

Despite promising EQE values, the PCE values of the best porous devices have been disappointing compared to those achieved using the same polymers in polymer–fullerene blends. The main factors limiting performance include: incomplete penetration of polymer into the voids of the porous film; sub-optimum nanostructure morphology where too little of the polymer volume lies within an exciton-diffusion length of the interface; poor charge transport in the porous metal oxide component; and a less than optimum photovoltage (as a result of an unnecessarily large driving force for interfacial charge separation). These factors, and strategies to address them, will be discussed in turn in the following sections.

Polymer infiltration

The degree of infiltration of polymer solution into the pores of a porous metal oxide film is influenced by several factors: the molecular weight of the polymer and its tendency to crystallise; the pore size, shape and depth, porous film thickness, solvent, drying conditions, and the surface-interaction energy of the two materials (*e.g.* their relative hydrophilicity). Infiltration can be monitored from the relative photoinduced transient absorption, due to separated charges, for illumination from the two sides of a porous film that has been coated with a polymer film that is thin enough to be incorporated into the pores. Different absorbance values for front and back illumination indicate that some of the polymer layer has not been incorporated.[17] Unquenched photoluminescence from the polymer side is another qualitative indicator of poor infiltration. Crystalline polymers such as P3HT can be particularly hard to incorporate.[29]

Among strategies used to encourage polymer infiltration are the uses of polymers possessing a liquid-crystal phase, which can be "melt processed" by heating above the liquid-crystal phase-transition temperature. The positive effect of this strategy has been demonstrated using a fluorene–bithiophene copolymer (F8T2) on porous TiO_2, although the effect is most pronounced only for thick films (Fig. 6).

Another strategy is the use of polymers with polar side groups: in the case of solid dye-sensitised solar cells, inert polymers of high ($\sim$100 000) molecular weight successfully infiltrate into micron-thick nanocrystalline TiO_2 films, apparently aided by the affinity between the polar polymer units and the polar TiO_2 surface.[30] An alternative approach to the problem is to disguise the polar surface of TiO_2 by coating the oxide with an amphiphilic molecular monolayer, such that the outward facing part of the attached molecule is non polar. Such a strategy (typically using silicon-based molecules) is commonly used to improve the compatibility of ITO substrates with organic films for thin film transistors. In the case of ZnO–polymer porous structures, an amphiphilic dye has been used to improve the compatibility of the metal oxide with P3HT.[31]

A quite different approach to the problem is to "grow" one material inside the other. van Hal and co-workers prepared a networked TiO_2 structure within a polymer matrix by co-depositing a TiO_2 precursor material from solution along with the polymer, and then converting the precursor to solid TiO_2 by a hydrothermal treatment.[32] Although efficient photo-induced charge separation and promising photocurrent generation could be obtained, the connectivity of the resulting TiO_2 network was hard to control, leading to disappointing performance possibly limited by poor charge transport.[33] The use of precursor to produce ZnO–polymer composites was more successful, leading to devices with external quantum efficiency values of over 25% and power-conversion efficiencies of around 1%.[34] An alternative approach is to grow the organic layer inside the porous oxide film, this can be achieved by *in situ* conversion of a soluble precursor to the conjugated component. Frechet and co-workers achieved P3HT infiltration by *in situ* cross-linking of a thiophene precursor possessing carboxylate groups for attachment to the TiO_2 surface.[35] Pre-treatment of the porous film with a dilute polymer solution ("dip-coating") can also assist infiltration.[17]

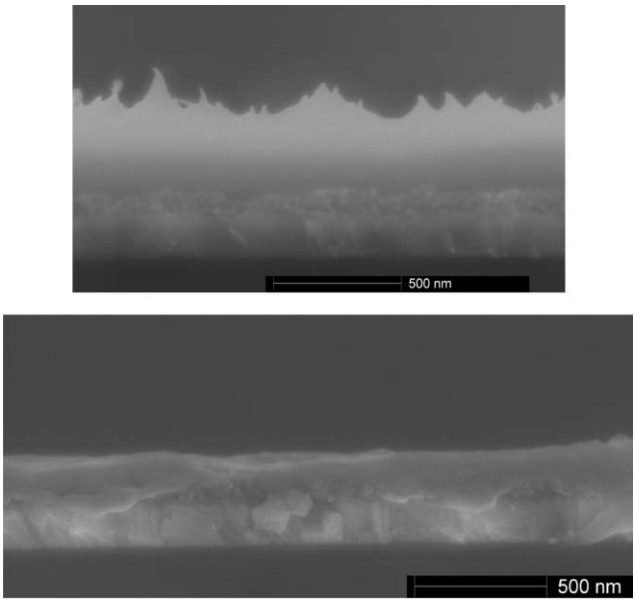

Fig. 6 Cross-sectional SEM images of porous TiO_2 coated with a layer of F8T2 polymer before (top) and after (bottom) thermal annealing above the liquid-crystal phase-transition temperature of the polymer.

Morphology

The first porous films studied were made by sintering of isotropic, colloidal TiO_2 nanoparticles into a connected thin film. The resulting irregular morphology is not ideal either for infiltration of organic material (*e.g.* because of inaccessible internal voids) or for ease of charge transport through either component. It is widely asserted that the ideal bulk heterojunction structure is one containing interdigitated vertical channels of donor and acceptor material, of width comparable to the exciton-diffusion length in the material (see Fig. 1(a)). Such vertical channel structures can be achieved in porous structures either by definition of pores in the metal oxide during film growth by templating methods[29,36] (Fig. 7(a)) or by growth of vertically aligned metal oxide rods (Fig. 7(b)). Although well-defined vertical pore structures have been demonstrated in TiO_2,[36,37] hybrid polymer–metal oxide PV

cells made from these have not yet outperformed the conventional porous structures, possibly because of penetration or electrode selectivity. Devices based on vertically aligned nanorods arrays have been promising in the case of ZnO nanorods, which can be prepared by sol gel methods in a range of dimensions.[38] Groups at NREL[39] and Imperial College London[31] have demonstrated EQE values of over 15% for P3HT–ZnO nano-rod devices. Comparison with devices based on ZnO nanoparticles of similar diameter showed superior performance for the nanorod devices, apparently due in part to slower interfacial charge recombination in the nanorods than in the particles (Fig. 7(b)).[31] These polymer–ZnO rod devices have so far been limited by the relatively large rod diameters and correspondingly large pore volumes, which limit the efficiency of exciton dissociation, and by the quality of the ZnO hole-blocking layers. Vertically aligned TiO_2 nanorods and nanotube arrays have been demonstrated and used in dye-sensitised solar cells;[40] such arrays are clearly of great interest for hybrid devices.

Charge separation and recombination

It is well known from studies of dye-sensitised solar cells that reducing the rate of interfacial charge recombination can result in better photovoltaic device performance.[41] Charge-recombination rates in polymer–porous TiO_2 structures at solar intensities are on the order of 100 μs for intimately combined materials. Reductions in interfacial recombination rate can be achieved by introducing a barrier layer to physically separate the electron and hole, or by modifying the energy-level alignment, and so the charge-transfer rate, at the interface. Barrier layers of insulating Al_2O_3 have been used successfully to suppress recombination in dye-sensitised solar cells, at no cost to the charge-separation yield provided that the overlayer thickness is optimised.[42] Preliminary studies on porous polymer–TiO_2 structures indicate that similar control of recombination rate is possible.[43] Coating with conjugated molecular monolayers can also control the rates of charge separation and recombination, for instance, by encouraging a cascade electron transfer from donor to metal oxide whilst blocking hole transfer.[31]

A different approach is to modulate the energy levels of the metal oxide relative to the organic donor by attaching a monolayer of permanent dipole moment molecules to the oxide surface. Depending on the sign of the dipole, the TiO_2 conduction band can be shifted up or down, so reducing or increasing the driving force for charge separation and reducing or increasing the recombination rate. An upward shift of the

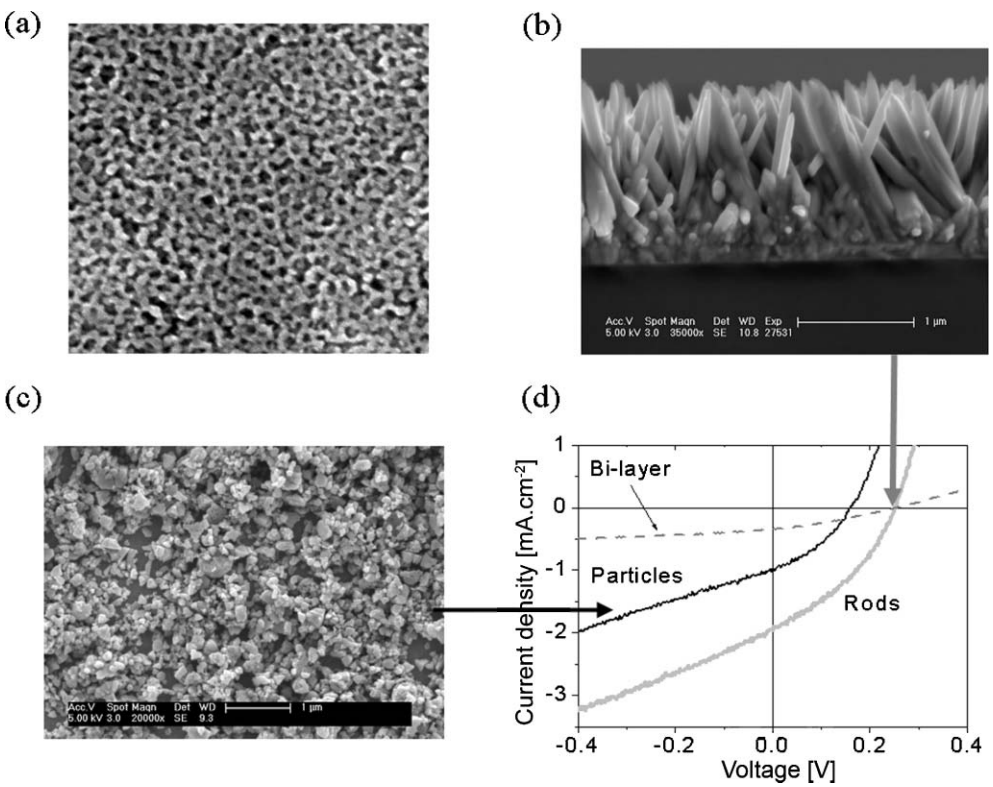

Fig. 7 (a) SEM images of pluronic templated TiO_2. Reprinted with permission from ref. 36. Copyright (2006) American Chemical Society. (b) Cross-sectional SEM image of film of vertically oriented ZnO nanorod; (c) SEM image (top view) of ZnO nanoparticle film; (d) Current density–voltage characteristics of hybrid P3HT–ZnO devices with different morphology. The device based on vertically oriented ZnO nanorods outperforms the device based on ZnO nanoparticles of similar diameter, while both nanostructured films outperform the bilayer. The device structure is ITO/dense ZnO (50 nm)/ZnO (~550 nm)/Z907/P3HT/PEDOT–PSS/Au in the case of the rod and particle devices, and ITO/dense ZnO (50 nm)/Z907/P3HT/PEDOT–PSS/Au for the dense layer only device. The superior performance of the ZnO nanorod-based film is attributed to the paths for charge transport, which are directed towards the electrodes. (b)–(d) Reprinted with permission from ref. 31. Copyright (2006) American Chemical Society.

TiO_2 conduction band edge is expected to increase the maximum open-circuit voltage (V_{oc}) available form the structure. The optimum structure would therefore have a driving force for charge separation that is just large enough to overcome the exciton-binding energy in the donor, so that near unit charge-transfer efficiency is achieved. In P3HT–TiO_2 structures, for example, the energy difference between the LUMO of P3HT (~ -3.1 eV) and the TiO_2 conduction band edge (~ -4.0 eV) is much larger than needed to drive exciton dissociation, and so large potential gains in V_{oc} could be made if the energy levels could be controlled. Preliminary studies of the effect of monolayers of differently substituted benzoic acids on porous polymer–TiO_2 structures and devices confirmed that the charge-transfer yield, and hence photocurrent, could be modulated using molecular monolayers according to the sign of the molecular dipole (Fig. 8). However, the effect of molecular modification was to increase V_{oc} for both signs of dipole, suggesting that the monolayer also has a (partial) barrier function, in suppressing recombination by spatially separating the charges. Protonation of the TiO_2 surface by covalently attached dyes or polymers can also be used to control the band-edge position.[44]

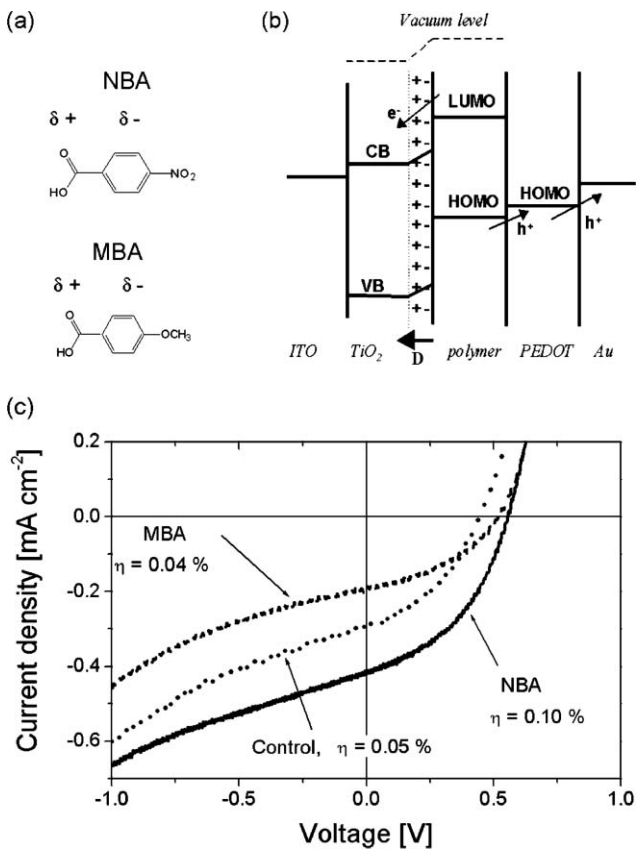

Fig. 8 (a) Chemical structures of the dipole molecules used, 4-methoxybenzoic acid (MBA) and 4–nitrobenzoic acid (NBA), (b) Proposed energy-level diagram for ITO/TiO_2/NBA/polymer/PEDOT–PSS/Au device, where D indicates the NBA dipole moment and e, h the directions of electron and hole transfer. (c) *J*–*V* Characteristics of ITO/TiO_2/dipole layer/polymer/PEDOT–PSS/Au devices under simulated AM1.5 irradiance, where the polymer used was poly[2-methoxy-5-(2-ethylhexyloxy)-1,4-phenylene-ethenylene-2,5-dioctyloxy-1,4-phenylene-ethenylene.

Transport

Several studies of porous polymer–TiO_2 structures[32,45] indicate that one of the factors limiting performance is the slow rate of charge transport within the nanocrystalline TiO_2. Intraparticle charge trapping in nanocrystalline TiO_2 is also known to limit charge transport in dye-sensitised solar cells.[46–48] Whilst replacing nanoparticles with vertically aligned TiO_2 nanorods may assist performance by defining the direction of charge transport (as discussed above) this may not eliminate the effect of trapping at intrinsic electron traps within the TiO_2 phase. An alternative route to improved electron transport is to replace the TiO_2 by an alternative oxide. ZnO is promising on account of high reported electron-transport properties in single-crystal nanorods.[38] However, one limitation on porous ZnO-based devices to date has been the metal oxide dense layer; ZnO dense layers appear to be less effective as hole-blocking layers than TiO_2, but dense TiO_2 layers cannot be used with ZnO porous layers because the higher conduction band edge of TiO_2 relative to ZnO means that TiO_2 impedes electron transfer from ZnO to the ITO electrode. Further optimisation of hole-blocking layers will resolve these problems. Tin oxide (SnO_2) offers high conductivity possibly due partly to good electron mobility; preliminary studies[49] have shown that porous SnO_2-based devices perform as well as porous TiO2-based devices, and that SnO_2 is a promising alternative for the metal oxide component in hybrid structures.

It should be noted that acceleration of charge transport is, in general, likely to accelerate charge recombination. Such a relationship has been established in the case of dye-sensitised solar cells.[47,50] In the case of bulk heterojunctions, however, segregation of domains of acceptor and donor material can reduce charge-recombination rates relative to the level expected for a transport-limited bimolecular process.[51] High mobilities and trap-free domains should also increase the probability of charges escaping the interface in hybrid bulk heterojunctions, and therefore fast transport may be expected to improve device performance.

Strategies to improve metal oxide–polymer blend films and devices

In the case of hybrid blend devices, despite the superior performance achieved so far relative to devices based on porous films, a different set of issues remain to be addressed before competitive hybrid photovoltaic cells can be developed. First, blending inorganic nanoparticles within organic conjugated polymers remains a challenge. Fine control of the phase segregation at the nanoscale requires the presence of capping agents, which prevent particle agglomeration, but are usually detrimental to exciton dissociation and charge transport.[7] Moreover, blend devices usually exhibit relatively low open-circuit voltages and fill factors compared with bilayer structures due to the presence of continuous pathways for either charge from top-to-bottom electrodes, enabling charge leakage. Another issue is that charge transport through the nanocrystal phase is highly sensitive both to the morphology and connectivity of that phase (which is hard to control), and to the presence of trap states within the nanoparticles. All

these aspects need to be addressed to improve device efficiency. In this paper, although we consider approaches to these challenges for the case of hybrid blend devices based on metal oxide nanoparticles such as ZnO[26,52] or TiO_2,[27,28] the strategies discussed are also relevant to II–VI nanoparticle based systems.

We will focus on the system based on the blend of TiO_2 nanorods (nc-TiO_2) and regioregular P3HT.[53] Here, the use of elongated particles synthesised through a non-hydrolytic route[54] in combination with a high mobility conjugated polymer (P3HT) is intended to give better insight into the key parameters controlling the device photophysics. In addition, the presence of an organic surfactant (trioctylphosphine oxide, TOPO) at the particle surface allows us to explore specific limitations on both charge recombination and transport.

TiO_2-nanorod properties and blend processing

The main advantage of a blend approach is the ease of producing a highly interpenetrating network of donor and acceptor materials from solution. To this end, nanocrystals of different nature are synthesised chemically from solution using specific surfactants. These ligands, such as TOPO[55] or oleic acid,[56] are usually required to disperse the hydrophilic nanoparticles in common apolar solvents used to dissolve the conjugated polymer. In the case of nc-TiO_2 with P3HT, thin film deposition by spin- or dip-coating from these initial mixtures leads to homogeneous blend morphologies, for particle content ranging from 20 to 80 vol% (Fig. 9).

The presence of an insulating ligand at the particle surface tends to reduce the efficiency of charge separation at the polymer–nanocrystal interface, as well as reducing electron-hopping rates between particles.[7] Strategies to overcome this problem include replacing the organic ligand at the nanocrystal surface using ligand-exchange procedures[22,57] and using a solvent combination that is capable of stabilising the ligand-free nanocrystals in solution[58] (in the case of ZnO, nanoparticles can be synthesised and mixed within some organic solvents without additional surfactant).[26] These additional steps make the blend processing more complex, but are of crucial importance to charge separation and transport.

Another strategy to improve the morphology of blend devices consists of using elongated nanocrystals such as rods[22,53,56,59] (see inset of Fig. 9(a)) through synthetic control of the nanocrystal shape. As in the case of II–VI tetrapods,[60] the aim is to improve electron transport in the electron-acceptor particle network by reducing the number of interparticle hops but without increasing domain sizes within the blend.[61]

Control of blend morphology through processing and solvent choice is also important in influencing phase intermixing and hence device function. For example, vertical phase segregation can be achieved by using high boiling-point solvents such as 1,2,4-trichlorobenzene, leading to improved transport perpendicular to the plane of the active layer.[23] Controlled assembly of nanocrystals deposited on an electrode prior to polymer deposition allows control over the heterojunction structure; this has been demonstrated for CdTe tetrapods.[62]

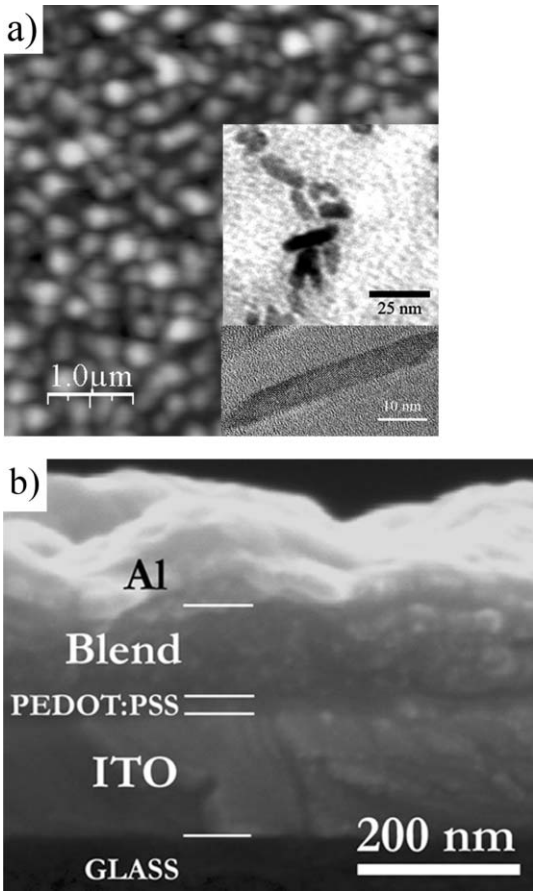

Fig. 9 (a) Atomic force microscopy picture of a typical blend film of P3HT incorporating 70 vol% of TOPO-capped TiO_2 nanorods. The height scale bar and root-mean-square roughness values are 130 and 20 nm, respectively. The insets present typical TOPO-capped TiO_2 nanorod morphologies. (b) Cross-sectional SEM image of the corresponding solar cell with the device structure: ITO/PEDOT–PSS/nc-TiO_2–P3HT Blend/Al.[53]

Charge separation and recombination in blend devices

Efficient photovoltaic energy conversion requires that the exciton, which is formed in the polymer phase following illumination of the device under solar conditions, reaches an interface and dissociates to generate free charge carriers that can reach their respective electrode before recombining. This process is typically limited by the exciton-diffusion length of organic semiconductors (5–15 nm). To overcome this limitation, the nanoparticle size, concentration and degree of phase segregation should be controlled to result in a large enough interface area between the two components. Fig. 10 illustrates the case of TOPO-capped nc-TiO_2 rods in P3HT as a function of the particle content.

Significant PL quenching is obtained at high particle content (Fig. 11(a)), consistent with efficient electron transfer from the P3HT phase to the metal oxide following excitation. The corresponding transient absorption signal, recorded using transient absorption spectroscopy (TAS),[63] shows the presence of relatively long-lived photoexcited charges (half life time of 100 μs) and a significant charge-separation yield that increases with TiO_2 content (Fig. 11(b)) (charge-separation yield is

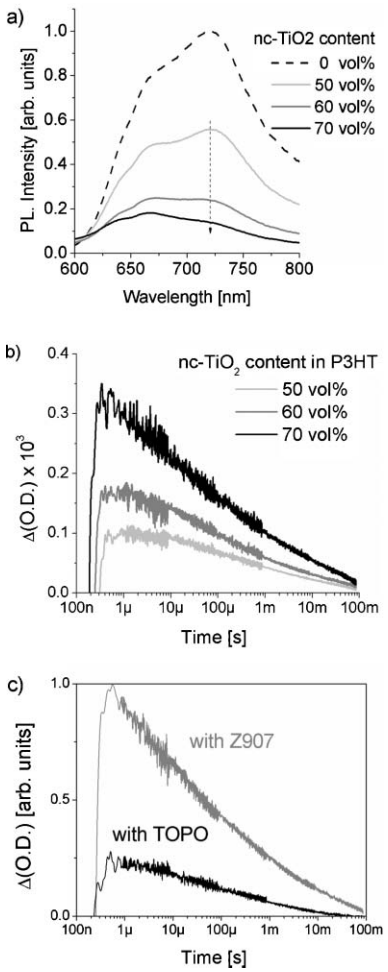

Fig. 10 (a) Photoluminescence spectra of TOPO-capped nc-TiO_2 nanorods–P3HT blends as a function of the particle content ranging from 50 to 70 vol% of nc-TiO_2 (excitation at 520 nm). (b) Transient absorption signals of the corresponding blends. The transient signal is recorded with λ_{pump} = 520 nm, P_{pump} = 40 μJ cm^{-2} per pulse and λ_{probe} = 950 nm. (c) Relative TAS signals of hybrid blends incorporating 70 vol% of TOPO-capped (black trace) and Z907-capped (grey trace) nc-TiO_2 rods.[53]

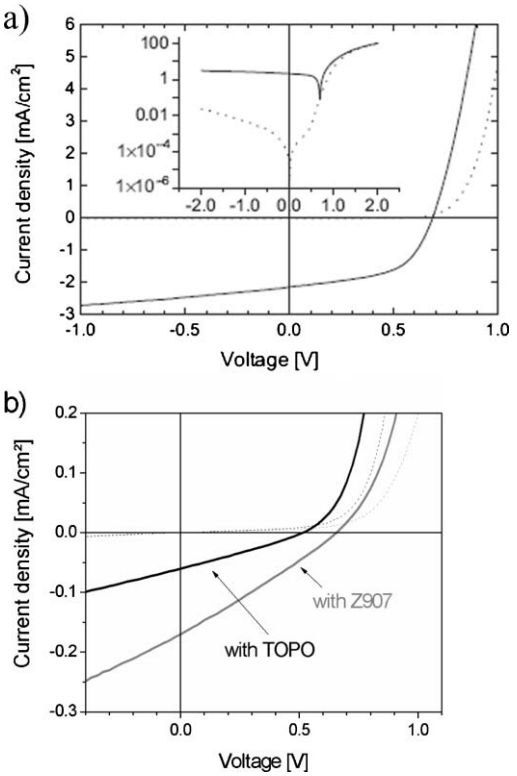

Fig. 11 (a) Current–voltage characteristics in the dark (dotted line) and under simulated solar illumination (75 mW cm^{-2}, solid line) of blend devices based on nc-ZnO (26 vol%) and P3HT. The inset shows a semi-logarithmic plot of the same curves. Reproduced with permission from ref. 52. Copyright Wiley-VCH Verlag GmbH & Co. KGaA. (b) Current – voltage characteristics in the dark (dotted lines) and under AM 1.5 solar conditions (40 mW.cm^{-2}, solid lines) of blend devices based on P3HT and either TOPO- (black lines) or Z907-capped (grey lines) nc-TiO_2 rods (60 vol.%). In both cases, the device structure is ITO/PEDOT:PSS/blend/Al.[53]

discussed further in ref. [53]). Fig. 11(c) demonstrates the influence of ligand type on charge-separation efficiency; by replacing a fraction of the TOPO molecules on the nanorod surface by the ruthenium-based dye Z907,[64] the TAS amplitude increases very significantly, in accordance with more efficient electron transfer through the ligand, possibly aided by the accessible LUMO level of the conjugated Z907 molecule compared to the insulating TOPO.[7,53]

Post-annealing treatments at low temperatures (50–150 °C) can also result in improved charge-transfer yields, and hence photocurrent generation. This was observed in P3HT–nc-TiO_2 blends upon annealing above the glass-transition temperature of the polymer.[53] Polymer-chain reorganisation evidently results in improved interfacial contact either through a slight displacement of the ligand or improved interpenetration of the phases.[53] Thermal annealing of P3HT–nanocrystal blends can also improve performance by increasing the charge mobility in the polymer phase.[52]

As in the case of porous metal oxide–polymer approaches, charge recombination and charge separation in blend devices are sensitive to the nature of the organic–inorganic interface and interfacial modification using dipole molecules, dyes, or insulating monolayers can also be applied to control the dynamics of photo-excited charges in blend systems. However, electronic transport between semiconducting nanocrystals limits the range of such strategies.

Transport

Charge transport in blend devices is determined both by the intrinsic charge-carrier mobilities in the donor and acceptor materials, and by the blend morphology. Effective percolation paths for both charges are required for efficient charge collection in the external circuit. Existence of such pathways depends upon both optimisation of particle content and nanocrystal shape. In this context, the use of elongated or three-dimensional nanocrystals can reduce the number of hopping events between isolated particles, leading to improved photocurrent generation.[22] However, the factors that control nanoparticle shape (*e.g.* choice of surfactant during growth) can also influence the nanoparticle packing in blend films, and

may lead to differences in film morphology, which also affect device performance. The dual control of particle solubility and blend morphology thus remains a key requirement for efficient device operation.

Intrinsic charge-carrier mobilities *within* nanoparticles (intraparticle transport) are sensitive to intrinsic electronic trap states. These may exist either within the nanoparticle, possibly enhanced by the high surface area to volume ratio of the small nanoparticles used[48,65] and are especially prevalent in astochiometric nanocrystals such as TiO_2,[53,66] or may be associated with surface-attached species. Although such defect states can reduce interfacial recombination rates, they are mainly detrimental to transport and hence to device performance. In this respect TiO_2-based systems differ from efficient blend systems based on CdSe quantum dots[22] or ZnO nanocrystals[52] (see Fig. 11(a)) where electronic states occupy the entire nanoparticle volume. More dispersive recombination kinetics are observed, accordingly, in blends of P3HT and TOPO-capped nc-TiO_2 than blends of P3HT and ligand-free ZnO rods.[67]

Transport *between* nanoparticles (interparticle transport) can be assisted by the choice of surface ligand. This effect is illustrated by comparing the device performance of P3HT-blend devices based on nc-TiO_2 rods capped with insulating TOPO ligands and with conjugated Z907-dye molecules (Fig. 11(b)). Further improvements in device performance require specific control of the nanocrystal-surface chemistry, and recent efforts, mainly applied on CdSe nanoparticles, have been observed in this direction.[57,68] Alternative approaches for improving charge transport consist of interconnecting the nanocrystals by sintering prior to polymer infiltration. Applying this procedure to nanocrystals as an alternative to co-deposition from a blend film provides a good model system for the study of connectivity effects in blend devices. Such an approach was successfully applied to colloidal nc-TiO_2-rod thin films, where annealing the nanoparticle thin films at 450 °C for 30 min under air resulted in organic ligand removal and particle sintering. Although this strategy requires the infiltration of a polymer in the resulting porous structure, preliminary results have shown that charge-carrier recombination is slower after sintering (1 ms) than before (100 μs) (Fig. 12), which is compatible with increased electron delocalisation and reduced trapping after sintering. The reduced recombination could potentially lead to increased open-circuit voltages.

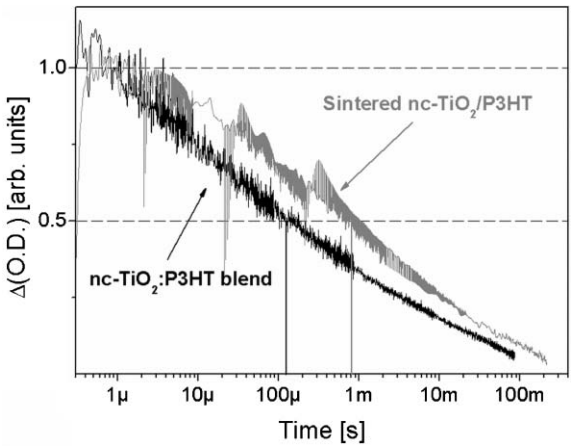

Fig. 12 Recombination kinetics probed by transient absorption spectroscopy (TAS) for different systems: TOPO-capped nc-TiO_2 rods–P3HT blends (black trace), sintered colloidal nc-TiO_2-rod film infiltrated by P3HT (dark grey trace) and bilayer structure dense TiO_2–P3HT (light grey trace). Corresponding half life time decays of ~100 μs, ~1 ms and ~10 ms, respectively, are materialised by vertical lines. The signals, which were recorded in similar experimental conditions (λ_{pump} = 520 nm, P_{pump} = 40 μJ^{-1} cm^{-2} per pulse, and λ_{probe} = 950 nm) are normalised in this graph.[53]

Device design

Whilst control of the organic–inorganic interface and the blend morphology are necessary to optimise charge separation and transport in polymer–nanoparticle blend systems, asymmetric electrodes are essential to ensure directional photocurrent and good device performance. Unlike porous polymer–metal oxide structures where directionality is built-in through the vertical stratification of components during fabrication, blend devices tend to present relatively low fill factors due to the presence of shunt pathways between the electrodes. On the other hand, blends offer more flexibility in electrode choice and the possibility of achieving higher open-circuit voltages by using electrodes of higher work-function difference. To improve selectivity, inorganic dense layers of the oxide, deposited by laser-spray pyrolysis, are good candidates to prevent direct collection of holes at the ITO electrodes. Use of a dense TiO_2 layer within a hybrid blend device resulted in a slight increase of the device fill factor,[69] for an ITO/dense TiO_2/blend/PEDOT–PSS/Au structure compared to an ITO/PEDOT–PSS/blend/Al structure, whilst the V_{oc} was larger for the latter. In another study, a compact TiO_2 nanorod interlayer between the TiO_2 nanorod–MEH–PPV blend films and the top aluminium electrode was found to increase photocurrent collection in a blend device, thus combining the high work-function difference and the electrode selectivity within the same structure (Fig. 13).[28]

Use of metal oxides in other organic photovoltaic devices

Although we have focused on the use of metal oxides as one of the active components in a bulk heterojunction solar cell, metal oxides have also found applications as components for light management or charge collection in organic solar cells. The high dielectric constant of TiO_2 (30–50) compared to organic materials means that thin layers of TiO_2 incorporated into an organic bulk heterojunction solar cell can influence the distribution of the optical field within the layered structure. Kim and co-workers used a thin layer of amorphous TiO_2 between the active polymer–fullerene layer and the top Al electrode. They attributed the resulting increase in photocurrent relative to a control sample with no TiO_2 to an improved optical field distribution whereby the optical absorption was shifted away from the metal contact where excitons which diffuse away from the donor/acceptor interface can be quenched.[70] Larger effects on light harvesting could be achieved, in principle, by using photonic band gap or grating

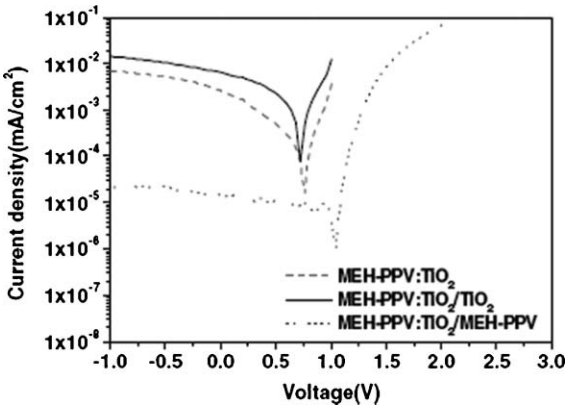

Fig. 13 Current–voltage characteristics of blend devices based on nc-TiO_2 rods (25 vol%) and MEH–PPV without (dashed line) or with an interlayer: either MEH–PPV (dotted line) or a compact nc-TiO_2-rods layer (solid line). The curves are recorded under monochromatic illumination at 560 nm (0.09 mW cm^{-2}). Reproduced with permission from ref. 28.

structures within the device to enhance the probability of absorption of red photons. Though photonic band-gap structures have not yet been applied to organic solar cells, inverse opal TiO_2 structures have been shown to enhance the EQE of dye-sensitised solar cells.[71] Through a simpler approach, the incorporation of (electronically inert) TiO_2 nanoparticles into an organic film has been shown to enhance light absorption *via* scattering.[72]

The influence of metal oxide dense layers on ITO electrode selectivity has been mentioned above. Dense TiO_2 layers are also attracting interest as potential electrodes for organic bulk heterojunction devices. Waldauf and co-workers managed to reduce shunt losses in a polymer–fullerene device by coating the ITO bottom contact with a layer of TiO_2 to make a selective electron-collecting electrode, and using PEDOT as a top contact.[73] A longer term goal is to use doped metal oxides as potential replacement for ITO, the most costly component in organic solar cells. Additionally, there has been some evidence that the stability of polymer–fullerene devices is enhanced when a TiO_2 layer is used as a hole-blocking layer.

Conclusion and outlook

Hybrid organic–metal oxide structures have attracted growing interest over the last five years as a model system within which to study the fundamental processes of charge separation and photocurrent generation in donor–acceptor heterojunctions. Although power-conversion efficiencies of the best hybrid photovoltaic devices are still low compared to the best polymer–fullerene structures, steady progress in performance has been made through growing understanding of the factors limiting performance and growing expertise in synthesis and control of materials. The hybrid systems illustrate very nicely the competing challenges faced in achieving a bulk heterojunction morphology that allows both efficient charge separation and efficient charge transport; they offer one of the most promising routes towards the ideal structure of vertically aligned interpenetrating donor and acceptor phases; and they have provided valuable understanding of the charge-transfer processes at the donor–acceptor interface. Moreover, expertise gained with hybrid systems has proved to be valuable in improving the performance of all organic photovoltaic systems.

Of the two types of polymer metal oxide structure reviewed here, porous and blend devices, blend structures have achieved the best photovoltaic performance so far, suggesting that the problems of interparticle transport can be overcome more easily than those of polymer infiltration. However, continuing improvements in molecular control of interfaces and in synthetic control of organised nanocrystal structures promise further advances with both approaches in the near future.

Acknowledgements

The authors are grateful to Dr Milo Shaffer and Dr Sabina Chyla for providing the TiO_2 nanocrystals used for the work in ref. 53, to Prof. James Durrant for the use of his transient absorption system, to Dr Ana Peiro for providing the ZnO rods used in ref. 31, and to Mrs Thilini Ishwara for preparing some samples for SEM measurements. We acknowledge useful discussions on various topics in this paper with Dr Jorg Ackermann of University of Marseille and with Prof. Donal Bradley, Prof. James Durrant, Dr Saif Haque, Mrs Thilini Ishwara, and Ms Martina Mohr and Dr Milo Shaffer of Imperial College London. Financial support from the UK Engineering and Physical Sciences Excitonic SUPERGEN programme is acknowledged. PR acknowledges the National Research Council, Sri Lanka for financial assistance.

References

1 J. J. M. Halls, C. A. Walsh, N. C. Greenham, E. A. Marseglia, R. H. Friend, S. C. Moratti and A. B. Holmes, *Nature*, 1995, **376**, 480.
2 G. Yu, J. Gao, J. C. Hummelen, F. Wudl and A. J. Heeger, *Science*, 1995, **270**, 1789.
3 G. Li, V. Shrotriya, J. S. Huang, Y. Yao, T. Moriarty, K. Emery and Y. Yang, *Nat. Mater.*, 2005, **4**, 864.
4 Y. Kim, S. Cook, S. M. Tuladhar, S. A. Choulis, J. Nelson, J. R. Durrant, D. D. C. Bradley, M. Giles, I. McCulloch, C. S. Ha and M. Ree, *Nat. Mater.*, 2006, **5**, 197.
5 M. M. Koetse, J. Sweelssen, K. T. Hoekerd, H. F. M. Schoo, S. C. Veenstra, J. M. Kroon, X. N. Yang and J. Loos, *Appl. Phys. Lett.*, 2006, **88**, 083504.
6 L. Schmidt-Mende, A. Fechtenkotter, K. Mullen, E. Moons, R. H. Friend and J. D. MacKenzie, *Science*, 2001, **293**, 1119.
7 N. C. Greenham, X. G. Peng and A. P. Alivisatos, *Phys. Rev. B*, 1996, **54**, 17628.
8 P. J. Alet, S. Palacin, P. R. I. Cabarrocas, B. Kalache, M. Firon and R. de Bettignies, *Eur. Phys. J.: Appl. Phys.*, 2006, **36**, 231.
9 N. Vlachopoulos, P. Liska, J. Augustynski and M. Gratzel, *J. Am. Chem. Soc.*, 1988, **110**, 1216.
10 B. C. O'Regan and M. Gratzel, *Nature*, 1991, **353**, 737.
11 T. J. Savenije, J. M. Warman and A. Goossens, *Chem. Phys. Lett.*, 1998, **287**, 148.
12 P. A. van Hal, M. P. T. Christiaans, M. M. Wienk, J. M. Kroon and R. A. Janssen, *J. Phys. Chem. B*, 1999, **103**, 4352.
13 A. C. Arango, S. A. Carter and P. J. Brock, *Appl. Phys. Lett.*, 1999, **74**, 1698.
14 N. A. Anderson, E. C. Hao, X. Ai, G. Hastings and T. Q. Lian, *Chem. Phys. Lett.*, 2001, **347**, 304.
15 A. C. Arango, L. R. Johnson, V. N. Bliznyuk, Z. Schlesinger, S. A. Carter and H. H. Horhold, *Adv. Mater.*, 2000, **12**, 1689.
16 J. S. Salafsky, *Phys. Rev. B*, 1999, **59**, 10885.
17 P. Ravirajan, S. A. Haque, J. R. Durrant, D. Poplavskyy, D. D. C. Bradley and J. Nelson, *J. Appl. Phys.*, 2004, **95**, 1473.

18 Q. Fan, B. McQuillin, D. D. C. Bradley, S. Whitelegg and A. B. Seddon, *Chem. Phys. Lett.*, 2001, **347**, 325.
19 P. Ravirajan, D. D. C. Bradley, J. Nelson, S. A. Haque, J. R. Durrant, H. J. P. Smit and J. M. Kroon, *Appl. Phys. Lett.*, 2005, **86**, 143101.
20 J. Nelson, J. Kirkpatrick and P. Ravirajan, *Phys. Rev. B*, 2004, **69**, 035337.
21 A. P. Alivisatos, *Science*, 1996, **271**, 933.
22 W. U. Huynh, J. J. Dittmer and A. P. Alivisatos, *Science*, 2002, **295**, 2425.
23 B. Sun, H. J. Snaith, A. S. Dhoot, S. Westenhoff and N. C. Greenham, *J. Appl. Phys.*, 2005, **97**, 014914.
24 P. Wang, A. Abrusci, H. M. P. Wong, M. Svensson, M. R. Andersson and N. C. Greenham, *Nano Lett.*, 2006, **6**, 1789.
25 D. Cui, J. Xu, T. Zhu, G. Paradee, S. Ashok and M. Gerhold, *Appl. Phys. Lett.*, 2006, **88**, 183111.
26 W. J. E. Beek, M. M. Wienk and R. A. J. Janssen, *Adv. Mater.*, 2004, **16**, 1009.
27 C. Y. Kwong, A. B. Djuri, P. C. Chui, K. W. Cheng and W. K. Chan, *Chem. Phys. Lett.*, 2004, **284**, 372.
28 T.-W. Zeng, Y.-Y. Lin, H.-H. Lo, C.-W. Chen, C.-H. Chen, S.-C. Liou, H.-Y. Huang and W.-F. Su, *Nanotechnology*, 2006, **17**, 5387.
29 K. M. Coakley and M. D. McGehee, *Appl. Phys. Lett.*, 2003, **83**, 3380.
30 A. F. Nogueira, J. R. Durrant and M. A. De Paoli, *Adv. Mater.*, 2001, **13**, 826.
31 P. Ravirajan, A. M. Peiro, M. K. Nazeeruddin, M. Graetzel, D. D. C. Bradley, J. R. Durrant and J. Nelson, *J. Phys. Chem. B*, 2006, **110**, 7635.
32 P. A. van Hal, M. M. Wienk, J. M. Kroon, V. J. H. Verhees, L. H. Slooff, W. J. H. van Gennip, P. Jonkheijm and R. A. J. Janssen, *Adv. Mater.*, 2003, **15**, 118.
33 L. H. Slooff, M. M. Wienk and J. M. Kroon, *Thin Solid Films*, 2004, **451–52**, 634.
34 W. J. E. Beek, L. H. Slooff, M. M. Wienk, J. M. Kroon and R. A. J. Janssen, *Adv. Funct. Mater.*, 2005, **15**, 1703.
35 J. S. Liu, E. N. Kadnikova, Y. X. Liu, M. D. McGehee and J. M. J. Frechet, *J. Am. Chem. Soc.*, 2004, **126**, 9486.
36 M. Zukalova, A. Zukal, L. Kavan, M. K. Nazeeruddin, P. Liska and M. Gratzel, *Nano Lett.*, 2005, **5**, 1789.
37 C. Goh, K. M. Coakley and M. D. McGehee, *Nano Lett.*, 2005, **5**, 1545.
38 M. Law, L. E. Grenne, J. C. Johnson, R. Saykally and P. D. Yang, *Nat. Mater.*, 2005, **4**, 455.
39 D. C. Olson, J. Piris, R. T. Collins, S. E. Shaheen and D. S. Ginley, *Thin Solid Films*, 2006, **496**, 26.
40 K. Zhu, N. R. Neale, A. Miedaner and A. J. Frank, *Nano Lett.*, 2007, **7**, 69.
41 J. R. Durrant, S. A. Haque and E. Palomares, *Coord. Chem. Rev.*, 2004, **248**, 1247.
42 E. Palomares, J. N. Clifford, S. A. Haque, T. Lutz and J. R. Durrant, *J. Am. Chem. Soc.*, 2003, **125**, 475.
43 T. Ishwara, P. Ravirajan and J. Nelson, to be published.
44 Y. X. Liu, S. R. Scully, M. D. McGehee, J. S. Liu, C. K. Luscombe, J. M. J. Frechet, S. E. Shaheen and D. S. Ginley, *J. Phys. Chem. B*, 2006, **110**, 3257.
45 P. Ravirajan, S. A. Haque, J. R. Durrant, D. D. C. Bradley and J. Nelson, *Adv. Funct. Mater.*, 2005, **15**, 609.
46 B. C. O'Regan, K. Bakker, J. Kroeze, H. Smit, P. Sommeling and J. R. Durrant, *J. Phys. Chem. B*, 2006, **110**, 17155.
47 J. Nelson, S. A. Haque, D. R. Klug and J. R. Durrant, *Phys. Rev. B*, 2001, **6320**, 205321.
48 N. Kopidakis, N. R. Neale, K. Zhu, J. van de Lagemaat and A. J. Frank, *Appl. Phys. Lett.*, 2005, **87**, 202106.
49 P. Ravirajan, Ph.D. Thesis, University of London, 2004.
50 N. Kopidakis, K. D. Benkstein, J. Van de Lagemaat and A. J. Frank, *J. Phys. Chem. B*, 2003, **107**, 11307.
51 A. Pivrikas, G. Juska, A. J. Mozer, M. Scharber, K. Arlauskas, N. S. Sariciftci, H. Stubb and R. Osterbacka, *Phys. Rev. Lett.*, 2005, **94**, 176806.
52 W. J. E. Beek, M. M. Wienk and R. A. J. Janssen, *Adv. Funct. Mater.*, 2006, **16**, 1112.
53 J. Bouclé, S. Chyla, M. S. P. Shaffer, J. R. Durrant, D. D. C. Bradley and J. Nelson, *Adv. Funct. Mater.*, 2007, submitted.
54 T. J. Trentler, T. E. Denler, J. F. Bertone, A. Agrawal and V. L. Colvin, *J. Am. Chem. Soc.*, 1999, **121**, 1613.
55 X. Peng, L. Manna, W. Yang, J. Wickham, E. Scher, A. Kadavanich and A. P. Alivisatos, *Nature*, 2000, **404**, 59.
56 A. Petrella, M. Tamborra, P. D. Cozzoli, M. L. Curri, M. Striccoli, P. Cosma, G. M. Farinola, F. Babudri, F. Naso and A. Agostiano, *Thin Solid Films*, 2004, **451–452**, 64.
57 C. Querner, P. Reiss, J. Bleuse and A. Pron, *J. Am. Chem. Soc.*, 2004, **126**, 11574.
58 W. U. Huynh, J. J. Dittmer, W. C. Libby, G. L. Whiting and A. P. Alivisatos, *Adv. Funct. Mater.*, 2003, **13**, 73.
59 W. J. E. Beek, M. M. Wienk, M. Kemerink, X. Yang and R. A. J. Janssen, *J. Phys. Chem. B*, 2005, **109**, 9505.
60 Y. Li, H. Zhong, R. Li, Y. Zhou, C. Yang and Y. Li, *Adv. Funct. Mater.*, 2006, **16**, 1705.
61 W. U. Huynh, J. J. Dittmer, N. Teclemariam, D. J. Milliron, A. P. Alivisatos and K. W. J. Barnham, *Phys. Rev. B*, 2003, **67**, 115326.
62 I. Gur, N. A. Fromer and A. P. Alivisatos, *J. Phys. Chem. B*, 2006, **110**, 25543.
63 Y. Tachibana, J. E. Moser, M. Grätzel, D. R. Klug and J. R. Durrant, *J. Phys. Chem.*, 1996, **100**, 20056.
64 P. Wang, S. M. Zakeeruddin, P. Comte, R. Charvet, R. Humphry-Baker and M. Gratzel, *J. Phys. Chem. B*, 2003, **107**, 14336.
65 K. Zhu, N. Kopidakis, N. R. Neale, J. van de Lagemaat and A. J. Frank, *J. Phys. Chem. B*, 2006, **110**, 25174.
66 J. Z. Zhang, *J. Phys. Chem. B*, 2000, **104**, 7239.
67 J. Ackermann and J. Bouclé, to be published.
68 D. Aldakov, F. Chandezon, R. De Bettignies, M. Firon, P. Reiss and A. Pron, *Eur. Phys. J.: Appl. Phys.*, 2007, **36**, 261.
69 J. A. Bouclé, S. Chyla, M. S. P. Shaffer, J. R. Durrant, D. D. C. Bradley and J. Nelson, to be published.
70 J. Y. Kim, S. H. Kim, H. H. Lee, K. Lee, W. L. Ma, X. Gong and A. J. Heeger, *Adv. Mater.*, 2006, **18**, 572.
71 S. Nishimura, V. Abrams, B. A. Lewis, L. Halaoui, T. E. Mallouk, K. D. Benkstein, J. Lagemaat and A. J. Frank, *J. Am. Chem. Soc.*, 2003, **125**, 6306.
72 Y.-G. Kim, J. Kim, H. Ahn, B. Kang, C. Sung, L. A. Samuelson and J. Kumar, *J. Macromol. Sci. A., Pure Appl. Chem.*, 2003, **40**, 1307.
73 C. Waldauf, M. Morana, P. Denk, P. Schilinsky, K. M. Coakley, C. Brabec and S. A. Choulis, *Appl. Phys. Lett.*, 2007, **89**, 233517.